Targeted Disruption of Pancreatic-Derived Factor (PANDER, FAM3B) Impairs Pancreatic β-Cell Function

Claudia E. Robert-Cooperman,[1] Jason R. Carnegie,[1] Camella G. Wilson,[2] Jichun Yang,[3] Joshua R. Cook,[2] Jianmei Wu,[1] Robert A. Young,[1] Bryan A. Wolf,[1,2] and Brant R. Burkhardt[1]

OBJECTIVE—Pancreatic-derived factor (PANDER, FAM3B) is a pancreatic islet-specific cytokine-like protein that is secreted from β-cells upon glucose stimulation. The biological function of PANDER is unknown, and to address this we generated and characterized a PANDER knockout mouse.

RESEARCH DESIGN AND METHODS—To generate the PANDER knockout mouse, the *PANDER* gene was disrupted and its expression was inhibited by homologous recombination via replacement of the first two exons, secretion signal peptide and transcriptional start site, with the neomycin gene. PANDER$^{-/-}$ mice were then phenotyped by a number of in vitro and in vivo tests to evaluate potential effects on glucose regulation, insulin sensitivity, and β-cell morphology and function.

RESULTS—Glucose tolerance tests demonstrated significantly higher blood glucose levels in PANDER$^{-/-}$ versus wild-type male mice. To identify the mechanism of the glucose intolerance, insulin sensitivity and pancreatic β-cell function were examined. Hyperinsulinemic-euglycemic clamps and insulin tolerance testing showed similar insulin sensitivity for both the PANDER$^{-/-}$ and wild-type mice. The in vivo insulin response following intraperitoneal glucose injection surprisingly produced significantly higher insulin levels in the PANDER$^{-/-}$ mice, whereas insulin release was blunted with arginine administration. Islet perifusion and calcium imaging studies showed abnormal responses of the PANDER$^{-/-}$ islets to glucose stimulation. In contrast, neither islet architecture nor insulin content was impacted by the loss of PANDER. Interestingly, the elevated insulin levels identified in vivo were attributed to decreased hepatic insulin clearance in the PANDER$^{-/-}$ islets. Taken together, these results demonstrated decreased pancreatic β-cell function in the PANDER$^{-/-}$ mouse.

CONCLUSIONS—These results support a potential role of PANDER in the pancreatic β-cell for regulation or facilitation of insulin secretion. ***Diabetes*** **59:2209–2218, 2010**

Pancreatic-derived factor (PANDER, FAM3B) is a 235–amino acid protein secreted predominantly from pancreatic α- and β-cells that appears to colocalize with both insulin and glucagon (1,2). The initial discovery of PANDER was the result of a computational algorithm, ostensible recognition of folds (ORF), in an attempt to identify novel cytokines based on the prediction of secondary structure. From ORF, it was hypothesized that the secondary structure of PANDER contained a four-helix bundle with a typical up-up-down-down topology, also found in numerous cytokines.

Initial in vitro experiments evaluating the impact of PANDER on pancreatic islets demonstrated the induction of apoptosis in primary islets (mouse, human, and rat) or islet-derived cell lines either by exogenous recombinant protein application or intracellular adenoviral delivery via a caspase-3–dependent mediated mechanism (2–4). Furthermore, microarray analysis of PANDER-treated islets demonstrated the activation of various cell death pathways via both caspase-3 and cyclin-dependent kinase inhibitor 1A (p21) (5). However, despite these in vitro results demonstrating a potential role for PANDER in islet apoptosis, our first animal model exploring the function of PANDER did not recapitulate these findings.

Transgenic mice that have pancreatic-duodenal homeobox-1 (PDX-1)–driven targeted overexpression of PANDER, specifically in pancreatic β-cells, display normal β-cell mass and function, but exhibit a glucose-intolerant phenotype after a high-fat diet (6). The mechanism of this observed glucose intolerance is still being elucidated. However, the liver is a potential target for PANDER and may be central to the observed glucose intolerance (7). Iodinated recombinant PANDER has been shown to bind to liver membranes. Pretreatment of liver-derived HepG2 cells with PANDER resulted in significant inhibition of insulin-stimulated activation of the insulin receptor, insulin receptor substrate-1, phosphatidylinositol-3′-OH-kinase (PI-3 kinase), and Akt, indicating the potential involvement of PANDER in regulation of hepatic insulin-signaling pathways.

Further evidence of PANDER's potential role in regulating glycemia has been generated by the influence of glucose on PANDER expression. Glucose has been demonstrated to *1*) increase secretion of cleaved PANDER and production of full-length PANDER in both insulinoma cells and primary islets (8), *2*) upregulate PANDER mRNA (9), and *3*) induce promoter activity (10). In addition, the critical pancreatic β-cell–specific transcriptional factor of PDX-1 binds to the PANDER promoter (11). Glucose has been demonstrated to induce *PANDER* gene expression via multiple signaling pathways that include Ca^{2+} protein kinase A (PKA), extracellular signal–regulated kinase 1/2 (ERK-1/2), and cAMP-responsive element-binding protein (CREB), as well as Ca^{2+} protein kinase C (PKC) and CREB mechanisms (9). Furthermore, glucose-regulated *PANDER* gene expression in MIN6 cells is dependent on both PI-3 kinase– and reactive oxygen species–related pathways.

Much of the data surrounding PANDER certainly suggest a potential role in glucose homeostasis, but the lack of a knockout animal model has hindered the elucidation of the biological function of PANDER. To address this, we

From the [1]Department of Pathology and Laboratory Medicine, The Children's Hospital of Philadelphia Research Institute, Philadelphia, Pennsylvania; the [2]University of Pennsylvania School of Medicine, Philadelphia, Pennsylvania; and the [3]Department of Physiology and Pathophysiology, Peking University School of Basic Medical Sciences, Peking University Diabetes Center, Beijing, China.

Corresponding author: Brant R. Burkhardt, burkhardtb@email.chop.edu.

Received 20 October 2009 and accepted 14 June 2010. Published ahead of print at http://diabetes.diabetesjournals.org on 21 June 2010. DOI: 10.2337/db09-1552.

have for the first time generated and characterized a PANDER knockout mouse. Deletion of PANDER resulted in glucose intolerance with impaired insulin secretion, revealing an unpredicted role for PANDER in pancreatic β-cell function.

RESEARCH DESIGN AND METHODS

Construction of PANDER targeting vector and knockout mice. A mouse 129/Sv-genomic bacterial artificial chromosome clone containing 14 kb of the PANDER sequence with the flanking DNA of our potential targeted region was used as a template to create both the long and short arms of the targeting vector. An approximate 4.3-kb long-arm genomic fragment containing the PANDER promoter was amplified by forward primer 5′-GC*GGTACC*GCCCT GGCTGTTCTGGAACTAA-3′ and reverse primer 5′-GA*GGATCC*GACCCAGT GTGGTGCCAA-3′ and was cloned in opposite orientation of the neomycin gene using the *Kpn*I and *Bam*H1 sites within cloning site A of the OSDupDel (courtesy of Youhai Chen, University of Pennsylvania) plasmid (incorporated restriction sites are italicized) (Fig. 1*A*). The approximate 2.9-kb short-arm genomic fragment containing intron 2 of the *PANDER* gene was amplified with forward primer 5′-GG*CACGTG*CTGTCATTCAAGCATTGGGA-3′ and reverse primer 5′-GC*GCTAGC*CTTCAACAAATAGGGTTCTA-3′, and was cloned into the cloning site B using the *Pml*I and *Nhe*I sites, respectively. The thymidine kinase gene was inserted at the 3′ end of the short arm of the targeting vector for negative selection. This targeting vector was created to remove the first 54 amino acids of PANDER, encompassing the transcriptional and translational start site, secretion signal peptide, and helix A. From a total of 288 clones generated by the University of Pennsylvania Gene Targeting Core, 2 that were correctly recombined were identified by PCR . Correct insertion of the 5′ arm and replacement of a portion of the *PANDER* gene with neomycin was confirmed by PCR amplification using the forward primer located in the *PANDER* promoter region of 5′-CTTGTGATGGTGGATGCCCAGTT-3′ and the reverse primer located in the neomycin gene of 5′-CTTCCTCGTGCTTTACG GTATC-3′. Confirmation of the 3′ arm was performed with the forward primer located in the neomycin gene of 5′-CCGAATAGCCTCTCCACCCAA-3′ and reverse primer located in intron two of the *PANDER* gene of 5′-GCCACTGC CACTAAAGAAAGA-3′. Both primer sets were used under the following cycling conditions: 1 cycle at 94°C for 2 min, 35 cycles at 94°C for 30 s, 60°C for 30 s, and 68°C for 4 min and 30 s, followed by 1 cycle of 68°C for 5 min using Accuprime *Taq*DNA polymerase (Stratagene). Chimeric mice were produced by microinjection of the correctly targeted cell clone into E3.5 C57BL/6 blastocysts and transferred to pseudopregnant foster mothers. High percentage male chimeras (70% or greater) were then chosen for subsequent mating with C57BL/6 females, and germline transmission was confirmed by PCR as described above. Chimeras were subsequently generated from the targeted embryonic stem (ES) cells and bred to C57BL/6 mice with germ line transmission. PANDER$^{+/-}$ mice were subsequently bred to homogeneity, and genomic confirmation was performed by PCR using primers to encompass the entire targeted region. Primers used for this PCR confirmation are described above as the forward primer located in the 5′ *PANDER* promoter region and the reverse primer located in intron 2. PCR conditions were the same as described above with the exception of the extension cycle, which was increased from 68°C for 4 min and 30 s to 12 min. The wild-type *PANDER* gene resulted in a 12.1-kb product, and the recombinant *PANDER* knockout allele resulted in an 8.3-kb product. All mouse procedures adhered to protocols approved by the University of Pennsylvania and Children's Hospital of Philadelphia Institutional Animal Care and Use Committee.

Quantitative analysis of gene expression via RT-PCR. Various tissues were collected from PANDER$^{+/+}$, $^{+/-}$, and $^{-/-}$ mice and immediately snap frozen in RNAlater (Qiagen). RNA was then isolated using the RNeasy Kit (Qiagen) following the manufacturer's instructions. Purity and quantity of the isolated RNA was determined by the A_{260}/A_{280}. RT-PCR of the *PANDER* gene was performed as previously described (2). Primers for detection of various genes involved in glucose-stimulated insulin secretion were purchased commercially (Applied Biosystems). Relative levels of mRNA expression were normalized to β-actin or 18S rRNA and calculated using the $2^{-\Delta\Delta CT}$ method.

Immunoblotting. Pancreatic islets were isolated from mice using the standard collagenase method as previously described (2). Cell lysates were prepared, analyzed, and electrotransferred to polyvinylidine fluoride (PVDF) membrane as previously described (2). Detection was performed using a rabbit polyclonal PANDER antibody that was produced via Genomic Antibody Technology (Strategic Biosolutions). Immunoblots were incubated with primary antibody at a dilution of 1:1,000 in 1× Tris-buffered saline with Tween (TBST) (10 mmol/l Tris base, 100 mmol/l NaCl, 0.1% Tween-20, pH 7.5) and 2% blocking solution (GE Healthcare) at 4°C overnight. The membrane was washed five times with 10 ml 1× TBST, incubated in 1:20,000 peroxidase-conjugated donkey anti-rabbit antibody at room temperature for 1 h before washing as above and then developed with enhanced chemiluminescence. For confirmation of equivalent loaded protein, following the detection of the PANDER immunoblot, PVDF membrane was stripped with Restore Western Blot Stripping Buffer (Pierce Biotechnology) and reprobed using 1:500 β-actin antibody (sc-8432; Santa Cruz Biotechnology). Detection was performed using the enhanced chemiluminescence Western blotting detection reagents (GE Healthcare). Measurement of glucokinase (sc-7908) and Kir6.2 (sc-20809) expression in pancreatic islets was performed as described above.

Glucose/insulin tolerance and arginine stimulation tests. For glucose tolerance tests (GTTs), mice were fasted overnight (~16 h) and subsequently injected intraperitoneally with 2 grams of glucose (Fisher Scientific) per kilogram of body weight. Glucose levels were measured at 0, 15, 30, 60, 90, and 120 min with a Freestyle glucometer via tail vein blood sampling (~5 μl). Measurement of plasma insulin concentration during the GTT was performed by obtaining blood collected from the tail vein in a Microvette CB 300 (Sarstedt), followed by centrifugation for serum separation and collection. Sera samples were then frozen at −80°C prior to insulin content analysis. Plasma insulin levels were determined by using the Ultra Sensitive Mouse Insulin ELISA kit (Crystal Chem). For insulin tolerance tests, mice were fasted for 4 h and then injected intraperitoneally with 0.75 units of insulin (NovoLog) per kilogram of body weight. Glucose levels were measured as described above. For arginine stimulation tests, mice were fasted overnight and then injected intraperitoneally with 2 grams of arginine (Sigma) per kilogram of body weight. Blood glucose and serum insulin levels were obtained as described above.

Hyperinsulinemic-euglycemic clamp and hepatic glucose production calculation. Clamp studies were performed and calculations were determined by the University of Pennsylvania Mouse Phenotyping Core as previously described (12).

Islet perifusion studies. Islet perifusions were performed as previously described (3). In brief, freshly isolated and hand-picked murine islets (~100) were collected under a stereomicroscope, washed twice with Krebs-Ringer bicarbonate buffer (KRB), and loaded into a 13-mm chamber containing a nylon membrane filter held at 37°C in a water bath. Islets were first perifused with KRB containing 0 mmol/l glucose for 1 h followed by a run perifusion consisting of increasing glucose conditions. Insulin content of effluent fractions and islet lysate were determined by radioimmunoassay.

Immunofluorescence. Immunofluorescence was performed on pancreatic sections as described previously, using confocal microscopy (Leica Microsystems) (2). The following antibodies were used: guinea pig anti-insulin (1:200 dilution; Linco), mouse antiglucagon (1:200 dilution; R&D Systems), anti-guinea pig alexa-fluor488 (1:5,000; Invitrogen), and anti-mouse alexa594 (1:5,000; Invitrogen).

Calcium imaging of isolated pancreatic islets. Murine pancreatic islets were isolated as described above and cultured for 3 days in complete RPMI. Islets were pooled from three mice per each genotype and then loaded with 15 μmol/l fura-2 acetoxymethylester (fura-2AM) (Molecular Probes). Calcium imaging of the isolated islets was performed as described before (13). In brief, fura-2AM–loaded islets were then transferred to a perifusion chamber and placed on a homeothermic platform of an inverted Zeiss microscope for calcium evaluation with a 40× oil-immersion objective. Islets were then perifused with KRB at 37°C at a flow rate of 2 ml/min while increasing concentrations of glucose in KRB were applied with a terminal application of 30 mmol/l KCl. Intracellular calcium concentration was determined by the ratio of the excitation of fura-2AM at 334 nm to that at 380 nm. Emission was measured at 520 nm with an Attofluor Ratio Vision Software (BD Biosciences).

ATP and ADP assays. ATP and ADP content was measured from 100 isolated murine islets pooled from two mice per each genotype and then stimulated during static incubation with glucose as previously described (14).

Hepatic insulin clearance. For estimating insulin clearance, the ratio of C-peptide (ng/ml) over insulin (ng/ml) area under the curve (AUC) was calculated from the mean serum levels obtained during a GTT (described above) from multiple time points (0, 30, and 120 min post-intraperitoneal glucose injection). Insulin concentrations were calculated as described earlier, and C-peptide levels were determined using the Mouse C-Peptide II ELISA (ALPCO).

Measurement of glucagon-like peptide-1. Mice were fasted overnight (~16 h) and then exposed to a 4-h refeed in which chow was added back to respective cages, and the mice were allowed to feed ad libitum. After the refeeding period, mice were killed and blood was collected in a Microvette CB 300 (Sarstedt), followed by centrifugation for serum separation and collection. Sera samples were then frozen at −80°C prior to glucagon-like peptide-1 (GLP-1) analysis. Total GLP-1 levels were determined from 50 μl of sera using the GLP-1 (7–36 and 9–36) ELISA kit (ALPCO).

Statistical analysis. Data are presented as mean ± SEM. Statistical significance of differences between groups was analyzed by paired Student *t* test using programs resident to Graphpad Prism version 5.01. A *P* value less than 0.05 was considered statistically significant.

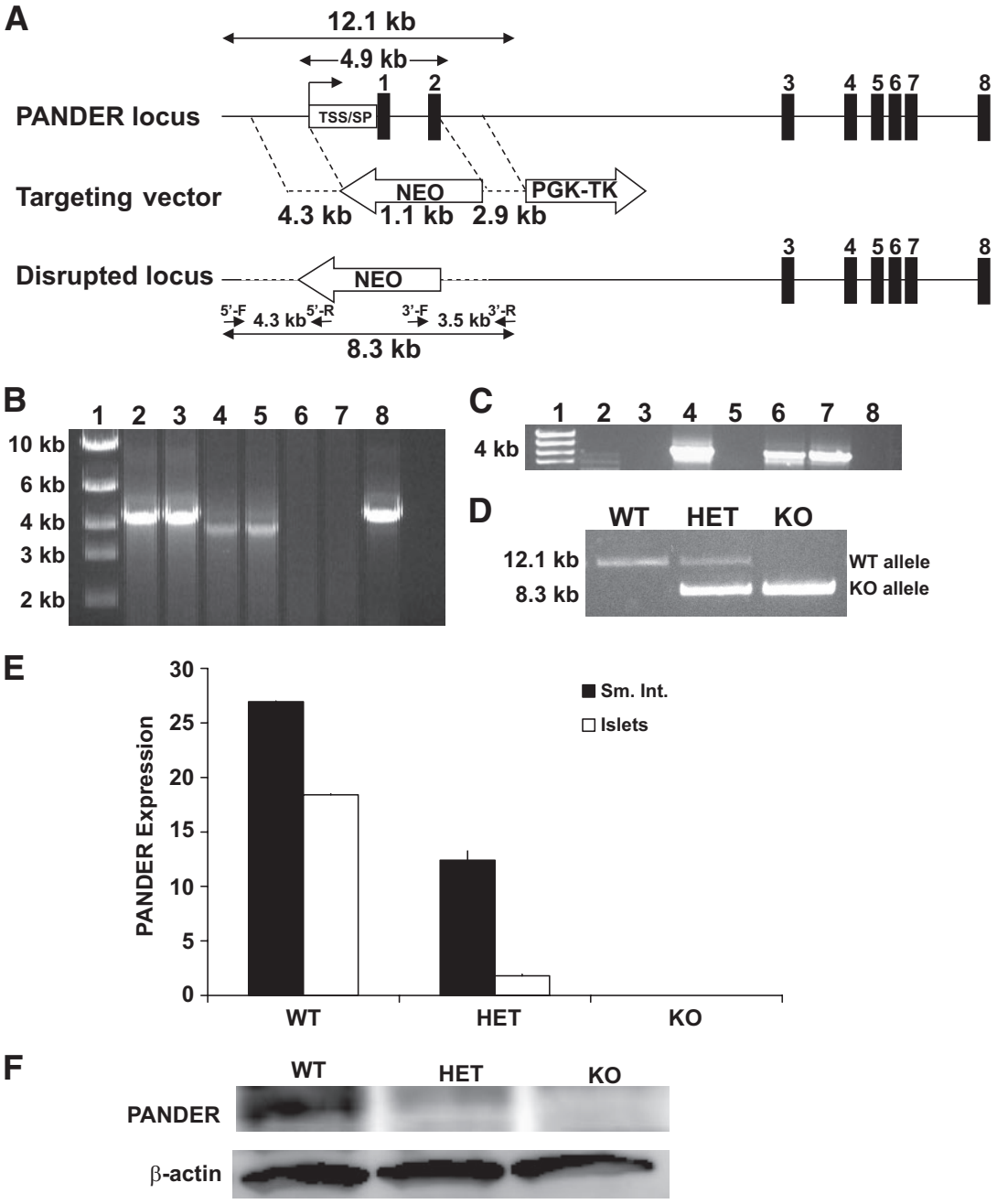

FIG. 1. Generation and confirmation of the PANDER knockout (KO) mouse. *A*: Schematic representation of genomic arrangement for mouse *PANDER* (*top*), targeting vector (*middle*), and the disrupted locus (*bottom*) produced by homologous recombination. The targeting vector was created by cloning a 4.3-kb long arm and 2.9-kb short arm of flanking *PANDER* genomic sequence surrounding the neomycin (*NEO*) gene in opposite orientation, intended to disrupt the transcriptional start site (TSS), secretion signal peptide (SP), and exons 1 and 2. Primers 5′-F/5′-R and 3′-F/3′-R were used for confirmation of correct gene targeting, resulting in a 4.3-kb and 3.5-kb product, respectively. Primers 5′-F/3′-R were used for routine PCR genotyping producing a 12.1-kb product for wild-type (WT), 12.1-kb/8.3-kb products for heterozygote (HET), and single 8.3 kb for KO. *B*: PCR analysis of genomic DNA extracted from transfected ES cells. Primer locations are shown in Fig. 1*A*. *Lane 1*: molecular marker; *lanes 2* and *3*: 4.3-kb arm amplified from two independent correctly targeted ES cell clones; *lanes 4* and *5*: 3.5-kb arm from correctly targeted ES cell clones; *lanes 6* and *7*: lack of 5′ and 3′ arm amplification from negative ES clones; and *lane 8*: 4.3-kb product from artificial template consisting of a plasmid containing the 5′ arm sequence with flanking nontargeted genomic regions. *C*: PCR confirmation of germline transmission. Genomic DNA was extracted from tail biopsies of mouse offspring with subsequent PCR using the 5′-F/5′-R primers. *Lane 1*: molecular marker; *lanes 2, 3, 5,* and *8*: mouse offspring negative for germline transmission; and *lanes 4, 6, 7*: mouse offspring with targeted PANDER deletion. *D*: Genotyping of mouse offspring. Representative PCR results are shown among WT, HET, and KO mice. *E*: RT-PCR analysis of RNA isolated from PANDER-positive tissues from WT, HET, and KO mice. *F*: Western evaluation of protein isolated from pancreatic islets for PANDER (top) and β-actin (bottom) expression from WT, HET, and KO mice.

RESULTS

Generation and confirmation of PANDER knockout mice. The *PANDER* gene was disrupted in ES cells by homologous recombination using a targeting vector that would replace the first two exons (54 amino acids), secretion signal peptide, and transcriptional start site with the neomycin gene inserted in the opposite orientation (Fig. 1*A*). Of the 288 ES clones, 2 were identified as correctly targeted (Fig. 1*B*) and used to generate chimeric male mice that passed the disrupted *PANDER* gene to the offspring (Fig. 1*C*). PANDER$^{+/-}$ mice were then bred to homogeneity to create PANDER$^{-/-}$ knockouts (Fig. 1*D*). To confirm the complete

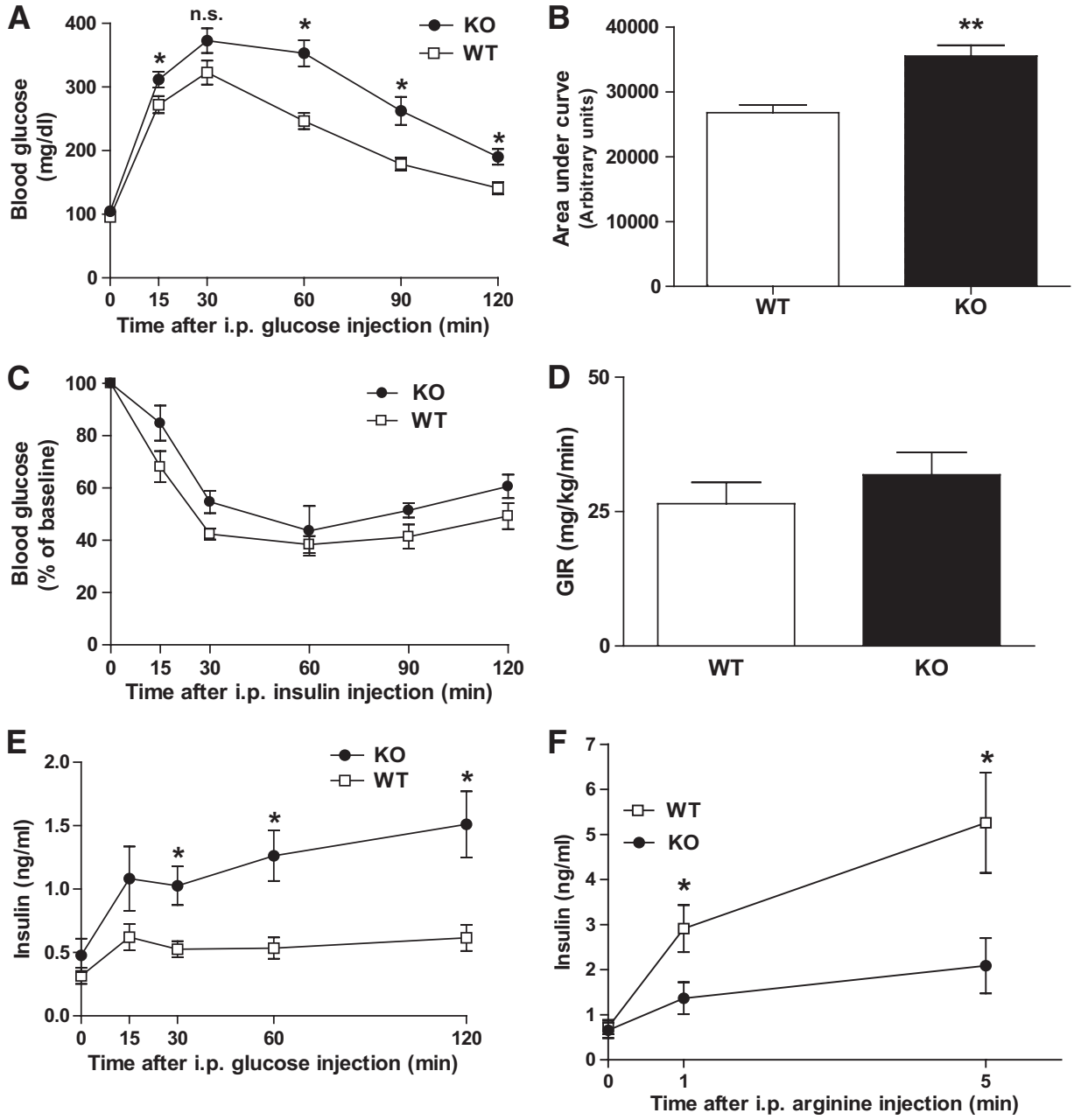

FIG. 2. Metabolic evaluation of PANDER$^{-/-}$ mice. *A*: Intraperitoneal GTT performed by injecting mice with glucose at 2 g/kg and measuring serum glucose concentration at the indicated time points (n = 14). *B*: AUC calculated from glycemic levels measured during the course of the GTT. *C*: Intraperitoneal insulin tolerance test performed by injecting mice with insulin at 0.75 units/kg and measuring glucose concentration at indicated time points (n = 8). *D*: Mean steady-state glucose infusion rate (GIR) during hyperinsulinemic-euglycemic clamp (n = 8). *E*: Measured insulin levels during GTT (n = 14). *F*: Intraperitoneal arginine tolerance test. Arginine was injected at 2 g/kg (n = 8–9). For all experiments above, male mice ~4–6 months old were evaluated. Values are means ± SE. *P < 0.05. **P < 0.01 by Student t test. n.s., not significant; KO, knockout; WT, wild-type.

absence of PANDER expression, particularly in the PANDER- restricted tissues of pancreatic islets and intestine, both RT-PCR and Western blot analysis were performed. PANDER mRNA expression was evaluated in the various PANDER-negative tissues of liver, spleen, kidney, and brain and in the PANDER-positive tissues of isolated pancreatic islets and small intestine. PANDER mRNA was not detected above background in both islets and small intestine from PANDER$^{-/-}$ mice, with marked reduction found in PANDER$^{+/-}$ mice (Fig. 1*E*). As expected, PANDER message was not detected in PANDER-negative tissues (data not shown). Western blot analysis of protein isolated from pancreatic islets of PANDER$^{-/-}$ mice demonstrated the absence of full-length PANDER protein, whereas a marked reduction was observed in heterozygotes (Fig. 1*F*).

Metabolic evaluation of PANDER$^{-/-}$ mice. PANDER$^{+/-}$ mice were intercrossed to generate a total of 233 offspring born with the expected Mendelian distribution with no observed increase in embryonic lethality (data not shown). There were no significant differences in size, appearance, or 24- or 48-h fasting levels of glucose, insulin, and glucagon among PANDER$^{+/+}$, $^{+/-}$, and $^{-/-}$ mice (data not shown). We initially evaluated the impact of PANDER deletion on glucose tolerance. GTTs demonstrated higher blood glucose levels in PANDER$^{-/-}$ versus wild-type 4- to 6-month-old male mice (Fig. 2*A*). Glucose

intolerance was also observed in younger 3-month-old male mice (data not shown). Glucose intolerance was not observed in littermate and genotype-matched females (data not shown). After glucose injection, the elevation in blood glucose levels was significantly higher in PANDER$^{-/-}$ mice compared with wild-type mice for a majority of the evaluated time-points, with a significant difference observed ($P < 0.001$) when determining total AUC for all glucose readings during the course of the GTT (Fig. 2*B*). The observed glucose intolerance may be attributed to either decreased peripheral insulin sensitivity or impaired glucose-stimulated insulin secretion (GSIS). To determine whether the observed glucose tolerance was the result of impaired insulin sensitivity, insulin tolerance tests and hyperinsulinemic-euglycemic clamps were performed. Both evaluations demonstrated similar insulin sensitivity for both the PANDER$^{-/-}$ and wild-type mice (Figs. 2*C* and *D*). Evaluation of GSIS was performed by measuring plasma insulin levels at various time points after glucose injection. Surprisingly, plasma insulin levels were significantly higher in PANDER$^{-/-}$ mice at the 30, 60, and 120 min time points (Fig. 2*E*). The lack of concordance between the observed result of glucose intolerance and higher insulin levels warranted further investigation. To further measure the in vivo insulin response of PANDER$^{-/-}$ murine islets, we performed administration of the nonglucose secretagog arginine. The acute insulin response (1–5 min after arginine injection) was significantly inhibited in the PANDER$^{-/-}$ mice (Fig. 2*F*). Overall, these findings indicate that PANDER serves a potential role in the maintenance of postprandial glucose homeostasis.

Decreased hepatic glucose production during hyperinsulinemic-euglycemic clamp in PANDER$^{-/-}$ mice. During the hyperinsulinemic-euglycemic clamp, hepatic glucose production (HGP) was evaluated (Fig. 3*A*). Basal HGP was similar between PANDER$^{-/-}$ and wild-type mice (72.6 ± 7.0 vs. 71.1 ± 7.5 mg/kg/min, respectively; P = NS). However, HGP in PANDER$^{-/-}$ mice was significantly lower than in wild-type mice during clamp conditions (18.6 ± 2.1 vs. 29.3 ± 4.2 mg/kg/min, respectively; $P < 0.05$). Percentage of HGP suppression during the clamp was concordantly higher in PANDER$^{-/-}$ mice but narrowly missed statistical significance (73.4 ± 3.0 vs. 53.3 ± 8.9%, respectively; $P = 0.05$) (Fig. 3*B*).

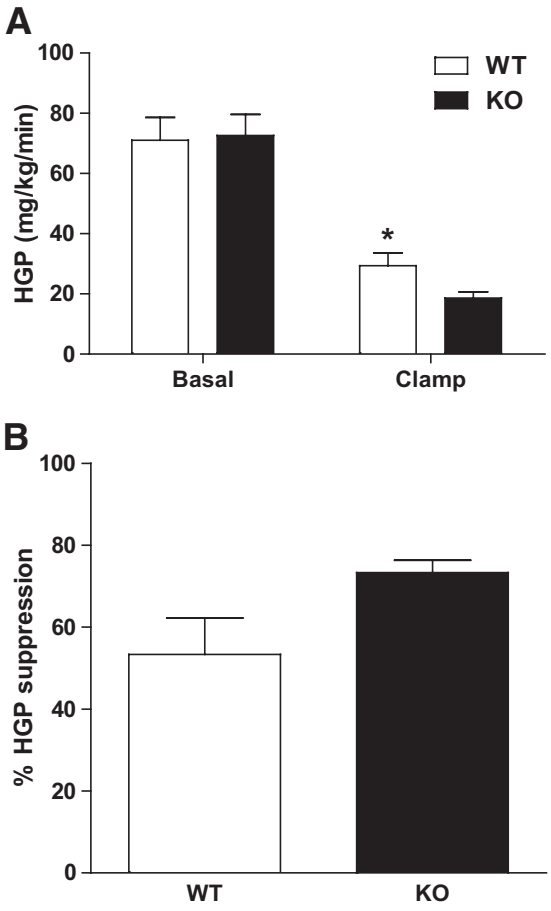

FIG. 3. HGP during hyperinsulinemic-euglycemic clamp is impaired in PANDER$^{-/-}$ mice. HPG during the hyperinsulinemic-euglycemic clamps was determined by subtracting the glucose infusion rate from the whole-body glucose appearance. Male mice ~5–7 months old were evaluated (n = 8). *A*: Basal HGP and production at the end of the hyperinsulinemic-euglycemic clamps. *B*: HGP suppression. Values are means ± SE. *$P < 0.05$ by Student t test. KO, knockout; WT, wild-type.

Loss of PANDER does not impact islet architecture or gene expression. Because neither insulin sensitivity nor HGP appeared to be the cause of the observed glucose intolerance, we next examined if the absence of PANDER in the pancreatic β-cell resulted in altered islet architecture or gene expression. Therefore, immunofluorescence was performed using antibodies recognizing the pancreatic hormones of glucagon and insulin to label the major islet cells of α- and β-cells, respectively (Fig. 4*A*). Both wild-type and PANDER$^{-/-}$ mice contained both pancreatic islet cell types, with insulin-positive β-cells localized to the core of the islet and the smaller glucagon-positive α-cell population localized to the mantle of the islet. Overall, immunofluorescent evaluation indicated no discernable difference in islet architecture. To evaluate any potential differences in mRNA expression for genes involved in GSIS, quantitative RT-PCR was performed on isolated pancreatic islet RNA (Fig. 4*B*). The measured islet genes are involved in multiple steps of GSIS and included glucose sensing and transport (GLUT2), glycolysis (glucokinase), K^+ channel (Kir6.2/Sur1), Ca^{2+} pumps (sarcoendoplasmic reticulum Ca^{2+} ATPase [SERCA]-2/3), and exocytosis (VAMP2, Rab3a, and Munc18c).

All of the genes were expressed at similar levels for wild-type and PANDER$^{-/-}$ islet RNA. Western blot analysis of isolated islets from PANDER knockout and wild-type mice revealed similar expression levels of GK and Kir6.2, despite the appearance of increased expression via RT-PCR (data not shown). Overall, intact islet architecture with similar islet gene expression in the absence of PANDER demonstrates that the observed glucose intolerance is unlikely to be attributable to impaired islet development and rather suggests the potential loss of β-cell function.

Inhibited GSIS from isolated islets of PANDER$^{-/-}$ mice. To further characterize islet function in isolation and separate from systemic effects, we performed insulin secretion studies on perifused islets isolated from both PANDER$^{-/-}$ and wild-type mice (Fig. 5*A*). Isolated islets were treated with increasing glucose concentrations ranging from 0–30 mmol/l glucose followed by depolarization with KCl stimulation. Wild-type islets produced a robust insulin secretory response to glucose. However, PANDER$^{-/-}$ islets displayed a significantly decreased insulin response to increasing concentrations of glucose compared with wild-type islets (1.0 ± 0.1 vs. 5.3 ± 1.7 AUC, respectively; $P < 0.05$) (Fig. 5*B*). Both wild-type and PANDER$^{-/-}$ islets

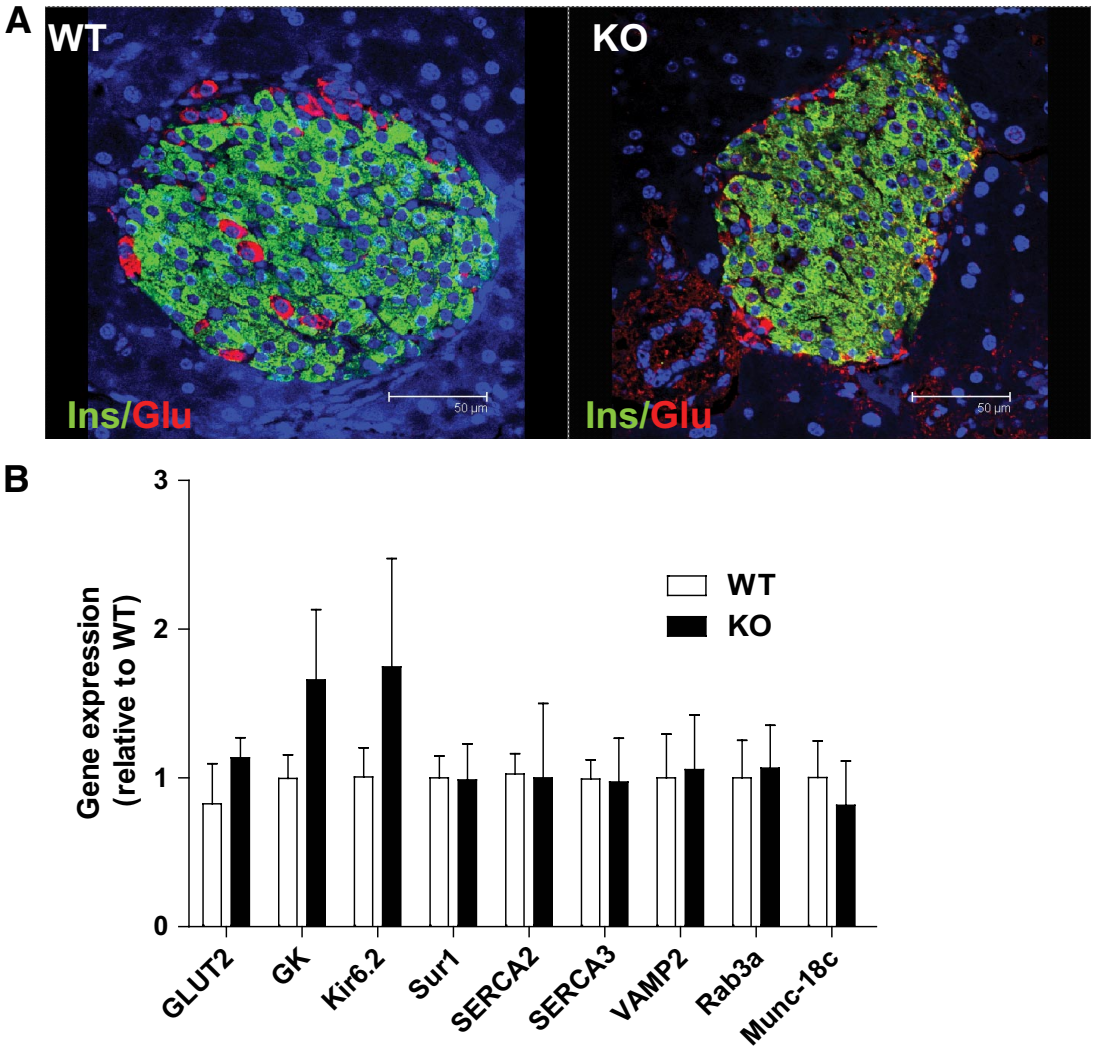

FIG. 4. Normal islet architecture and gene expression in PANDER$^{-/-}$ mice. Pancreatic sections from 4- to 6-month-old male mice were evaluated via immunofluorescence for detection of insulin (green) and glucagon (red). DAPI nuclear staining is shown in blue. *A*: Representative micrographs of insulin- and glucagon-labeled pancreatic sections from PANDER WT (*left panel*) and PANDER$^{-/-}$ mice (*right panel*), respectively. *B*: Gene expression analysis via RT-PCR in isolated islets of PANDER$^{-/-}$ and WT mice. Various genes involved in GSIS were evaluated in 5- to 7-month-old male mice (n = 3). Values are means ± SE. P = not significant for all genes as determined by Student t test. KO, knockout. (A high-quality digital representation of this figure is available in the online issue.)

responded similarly to depolarization via KCl at the conclusion of the experiment (1.7 ± 0.2 vs. 3.4 ± 1.1 AUC, respectively; P = NS) (Fig. 5*C*). To further characterize if the insulin secretory defect is attributed to decreased insulin production, insulin content was also measured from isolated islets (Fig. 5*D*). Insulin levels were equivalent in both wild-type and PANDER$^{-/-}$ islets (5,272 ± 1,311 vs. 7,565 ± 1,049 ng/ml/50 islets, respectively; P = NS). Together, these results suggest that PANDER impacts pancreatic β-cell function with a potential role in mediating GSIS.

PANDER-deficient islets display normal glucose metabolism with altered Ca^{2+} response to both glucose and KCl. The inhibited insulin secretion found in PANDER$^{-/-}$ islets did not appear to be based at the level of islet architecture, metabolic gene expression, or insulin content, and therefore suggested a potential disruption of glucose metabolism or generation of secondary signals required for initiating insulin exocytosis. To evaluate both glucose metabolism and generation of secondary signals, we measured the ATP-to-ADP ratio and intracellular Ca^{2+}, respectively, from both PANDER$^{-/-}$ and wild-type isolated islets. At physiological glucose concentrations (2, 5, and 10 mmol/l), the ATP-to-ADP ratio in PANDER$^{-/-}$ islets was indistinguishable from that of wild-type islets (data not shown). These results suggest that glucose metabolism is maintained in PANDER$^{-/-}$ islets, and this was consistent with the maintenance of normal gene expression of the various metabolic genes of GLUT2 and glucokinase. For evaluation of secondary signals, changes in cytosolic Ca^{2+} during glucose and KCl stimulation were monitored by fura-2 fluorescence imaging (Fig. 6). The intracellular Ca^{2+} response in PANDER$^{-/-}$ islets differed from that in wild-type islets in the following ways: hyperresponse of calcium at the 3-mmol/l condition; lack of calcium dip attributed to SERCA (15,16) immediately preceeding the rapid rise in intracellular calcium at 16 mmol/l glucose that was observed in wild-type islets; modest descrease in overall amplitude following 16 mmol/l glucose; and decreased KCl response. However, both PANDER$^{-/-}$ and wild-type islets promptly returned to baseline after reaching the 0-mmol/l

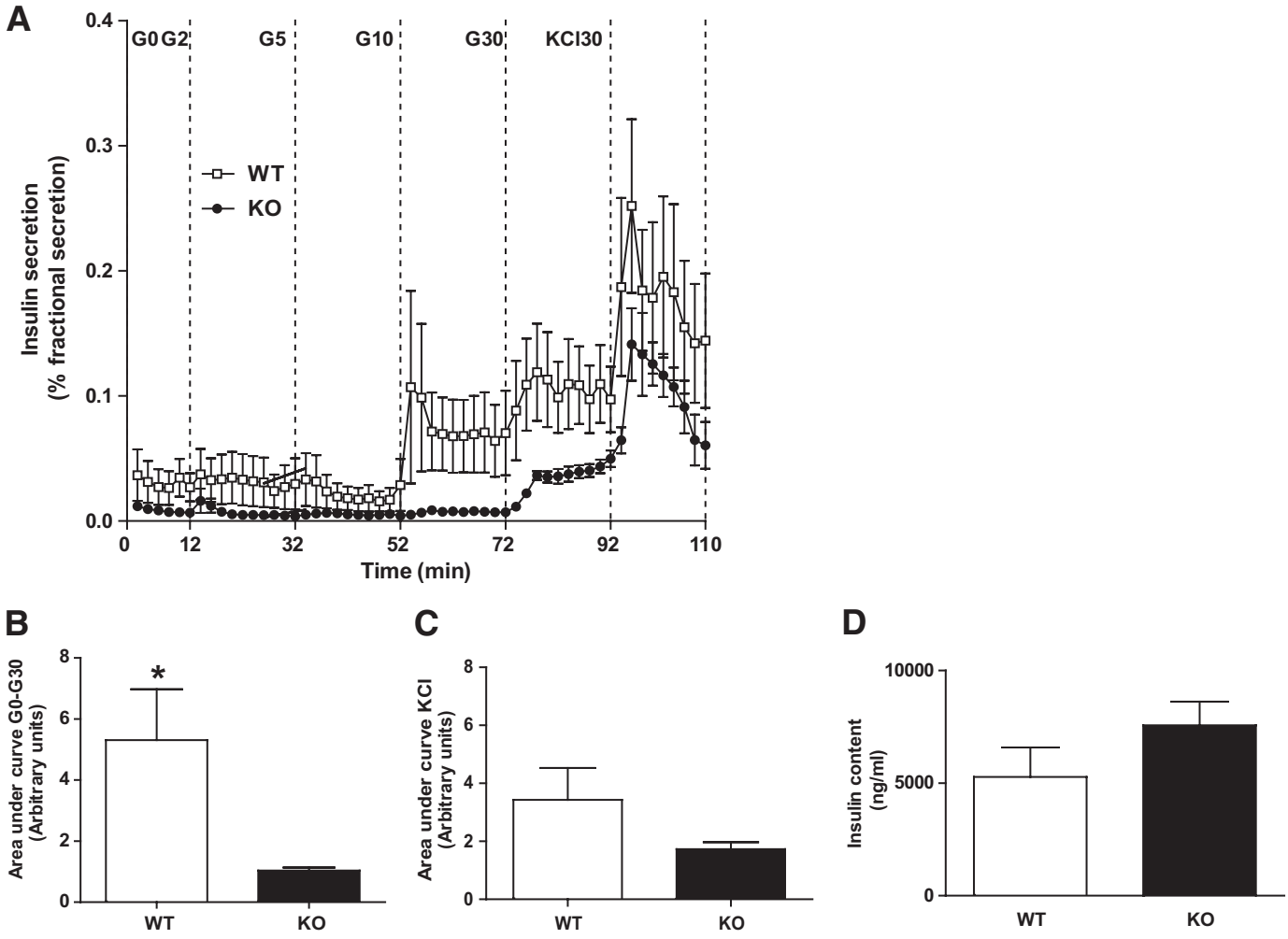

FIG. 5. Islet perifusions demonstrate impaired insulin secretion in PANDER$^{-/-}$ mice. *A*: Pancreatic islets were isolated and evaluated from male mice ~5–7 months old. Islets were isolated and incubated with increasing concentrations of glucose of 0 mmol/l (G0), 2 mmol/l (G2), 5 mmol/l (G5), 10 mmol/l (G10), and 30 mmol/l (G30) with a terminal step of 30 mmol/l KCl (KCl30) at indicated times. Time at which glucose condition was increased is shown above and noted on the *x*-axis. Effluent fractions were collected and insulin was measured by radioimmunoassay (n = 6–7). *B*: AUC calculated for insulin secretion from the G0 to the G30 condition. *C*: AUC determined for the insulin secretion during the KCl condition. *D*: After conclusion of the perifusion experiment, islets were collected and lysed with acid alcohol, and subsequent measurements of insulin concentrations were taken via radioimmunoassay. Values are means ± SE. *$P < 0.05$ by Student t test.

glucose condition. The abnormal calcium handling of PANDER$^{-/-}$ mouse islets may potentially indicate a mechanism for the impaired GSIS observed in vitro and glucose intolerance with blunted arginine response observed in vivo.

Decreased insulin clearance in PANDER$^{-/-}$ mice. The incongruity of the data indicating a defect in GSIS of the PANDER$^{-/-}$ islets with the otherwise higher levels of circulating insulin detected during the GTT potentially indicated altered insulin clearance, especially in the presence of normal insulin tolerance. C-peptide is cosecreted with insulin at equimolar amounts but, in contrast to insulin, passes the liver without considerable extraction with a half-life 10-fold higher than that of insulin (17,18). Therefore, many studies have evaluated insulin clearance based on the changes in C-peptide–to–insulin ratios determined at single or multiple time points (19,20). We used this same indirect approach to investigate potential alterations in hepatic insulin clearance (Fig. 7). Insulin and C-peptide concentrations increased robustly after glucose administration for both PANDER$^{-/-}$ and wild-type islets (Figs. 7*A* and *B*). However, as observed previously (Fig. 2*E*), insulin levels were higher in the PANDER$^{-/-}$ than in the wild-type mice (Fig. 7*A*). In contrast, C-peptide levels were initially higher in PANDER$^{-/-}$ mice, but then similar to wild-type mice after glucose stimulation (Fig. 7*B*). The overall C-peptide–to–insulin ratio was reduced significantly in PANDER$^{-/-}$ mice indicating a potential impairment in hepatic insulin clearance (Fig. 7*C*).

DISCUSSION

The biological function of PANDER has remained elusive since its initial discovery in 2002. Our previous reports and a publication from another research group suggested a potential role for PANDER in glucose homeostasis; however, the lack of a knockout mouse has hindered further biological evaluation. Our investigation has attempted to directly address this limitation via creation of a PANDER$^{-/-}$ mouse and to further establish a functional role for PANDER in the maintenance of glucose homeostasis.

Targeted disruption of PANDER did not result in increased embryonic lethality or gross morphological differences between PANDER$^{-/-}$, $^{+/-}$, or wild-type mice.

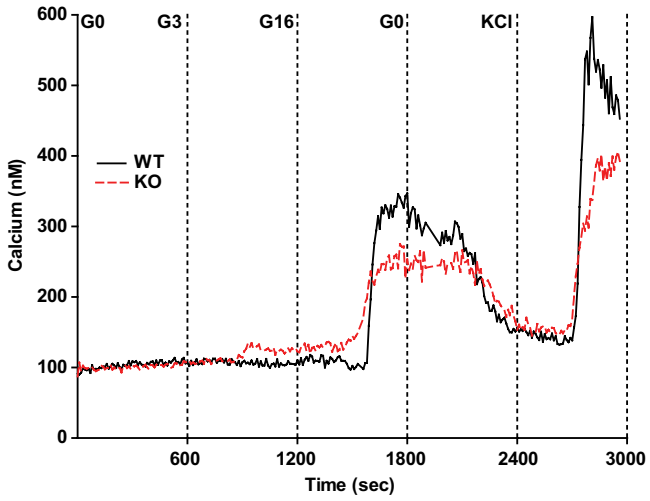

FIG. 6. Abnormal calcium response to glucose stimulation in PANDER$^{-/-}$ islets. Intracellular calcium concentration was determined via fura-2 fluorescence imaging during a glucose perifusion on isolated PANDER$^{-/-}$ and WT islets with stimulation from a glucose ramp and KCl (n = 3). Time of glucose increase is shown above and on the x-axis. Representative calcium plots are shown. Values are means ± SE.

However, PANDER$^{-/-}$ male mice displayed glucose intolerance, whereas littermate and genotype-matched females were indistinguishable. However, it is not unusual for a glucose-intolerant phenotype to be more severe in male versus female mouse models (21–23). Interestingly, our PANDER transgenic model also displays a male-specific phenotype (6). Deletion of PANDER did not appear to alter fasting levels of various hormones (i.e., insulin, glucagon, amylin, or leptin), and the metabolic defect occurred in the PANDER$^{-/-}$ mice during periods of nutrient challenge (i.e., glucose), suggesting that PANDER serves a putative role in regulating postprandial glucose homeostasis rather than maintaining basal normoglycemia.

PANDER$^{-/-}$ male mice are glucose intolerant. In addition, isolated islets appear to exhibit an insulin secretory defect in response to glucose (in vitro) and arginine (in vivo) and display an abnormal calcium response to both glucose and KCl. Indeed, it has been proposed that decreased GSIS can be attributed to abnormal Ca^{2+} handling of pancreatic islets, as has been reported in the islets obtained from the type 2 diabetic models of the Goto-Kakizaki and neonatal streptozotocin rats (24,25). An additional reported defect in Ca^{2+} handling has been the absence of the initial sequestration of Ca^{2+} by β-cell SERCA found in diabetic *db/db* murine islets (26). The initial Ca^{2+} dip after glucose stimulation is dependent on functional SERCA and appears to serve a critical role in GSIS. However, mRNA levels of SERCA 2/3 were similar between PANDER$^{-/-}$ and wild-type mice, but activity has yet to be evaluated. Overall, the defective Ca^{2+} handling observed in the PANDER$^{-/-}$ islets may provide a causative mechanism for the impaired GSIS.

A peculiar caveat to our results was discordance between the higher insulin levels found in vivo during the GTT and impaired insulin secretion in vitro in the PANDER$^{-/-}$ mice. Protective and compensatory mechanisms may exist in vivo that preserve and maintain β-cell function, whereas these defects are substantially exaggerated and identified in isolated islets. Also, circulating insulin levels not only reflect secretion but also clearance, and therefore suggest PANDER$^{-/-}$ mice may also have altered hepatic insulin clearance. Indeed, our model displayed decreased insulin clearance, which suggests that PANDER may have a role in impacting liver function. Alternatively, the decreased clearance may serve as a compensatory mechanism to counteract impaired insulin secretion. Interestingly, other knockout models have also demonstrated a similar phenotype of impaired β-cell function with in vivo hyperinsulinemia. The deletion of hepatocyte nuclear factor-4α (HNF-4α) in pancreatic β-cells resulted in hyperinsulinemia in fasted and fed mice but also demonstrated impaired glucose tolerance and abnormal responses of the isolated HNF-4α$^{-/-}$ islets by both islet perifusion and calcium imaging (27). In addition, the glucagon receptor knockout (Gcgr$^{-/-}$) mouse demonstrated higher insulin levels after a tail vein-injected glucose challenge, yet revealed a blunted glucose-stimulated insulin response in isolated islets at high glucose concentrations (28). In Gcgr$^{-/-}$ mice, the impaired GSIS was restored and enhanced due to increased levels of biologically active GLP-1. However, PANDER$^{-/-}$ did not demonstrate increased postprandial serum GLP-1 levels compared with wild-type mice (data not shown), which suggests that the incongruity of the observed defect in GSIS with the otherwise higher levels of circulating insulin detected during GTT may be the result of altered hepatic function. Although PANDER$^{-/-}$ mice display impaired GSIS, addi-

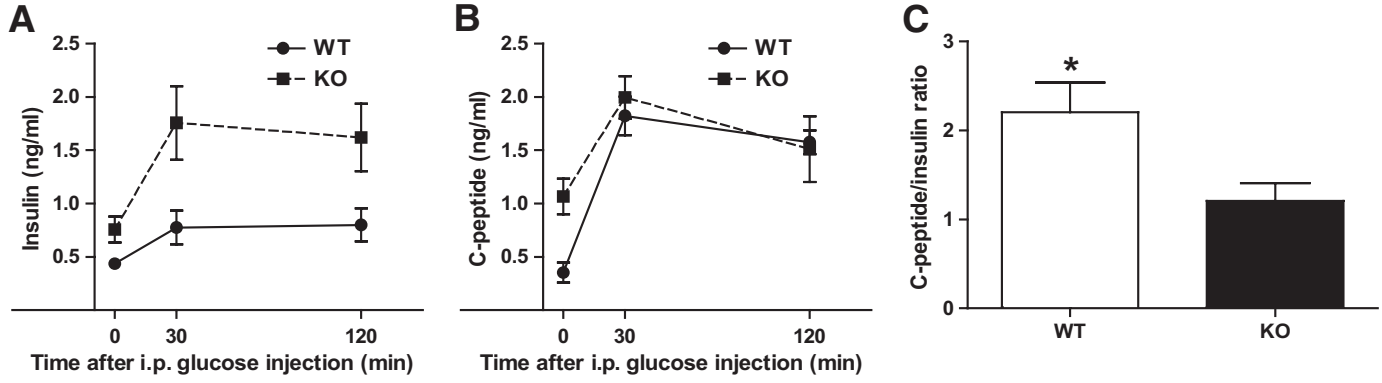

FIG. 7. Decreased insulin clearance in PANDER$^{-/-}$ mice. Intraperitoneal GTT performed by injecting mice with glucose at 2 g/kg and measuring serum insulin and C-peptide concentrations at the indicated time points. Male mice ~5–7 months old were evaluated (n = 3–6). Insulin (A) and C-peptide (B) serum concentrations were determined with commercially available ELISA (ALPCO). C: C-peptide–to–insulin ratio based on AUC calculated from glycemic levels of insulin and C-peptide measured during the course of the GTT. Values are means ± SE. *P < 0.05 by Student t test.

tional data are needed to substantiate that the deficiency in Ca^{2+} regulation of the pancreatic β-cell is causative of the insulin secretory defect, which is beyond the scope of this investigation. Further studies are needed to fully establish the role of PANDER in GSIS and the molecular mechanism responsible for impaired insulin secretion. The lack of our PANDER$^{-/-}$ model to develop overt diabetes or chronic hyperglycemia may be potentially attributed to PANDER serving multiple functions. The hyperinsulinemic-euglycemic clamp studies showed significantly decreased HGP and a strong trend in increased HGP suppression compared with wild-type mice. This result would directly oppose the glucose intolerance observed during the GTT and could be limiting the higher glycemic values observed during this assay. Previous literature showing that PANDER binds to liver membranes and putatively suppresses insulin action in conjunction with the PANDER transgenic model demonstrating increased HGP is very consistent with our findings in the PANDER$^{-/-}$. Our surprising result in the PANDER$^{-/-}$ mouse certainly suggests that PANDER may be serving multiple roles in regulating glucose levels via not only the liver but also through a direct involvement within the pancreatic islet in either regulation or facilitation of insulin secretion.

ACKNOWLEDGMENTS

This work was supported by grant K01-DK070744 (to B.R.B.) from the National Institute of Diabetes and Digestive and Kidney Diseases, National Institutes of Health, and the Juvenile Diabetes Research Foundation (to B.A.W.). This publication was made possible through core services provided by the Diabetes and Endocrinology Research Center at the University of Pennsylvania (DK19525).

No potential conflicts of interest relevant to this article were reported.

C.E.R.-C., J.R.Ca, C.G.W., and R.A.Y. researched data and reviewed/edited the manuscript. J.Y. and B.A.W. reviewed/edited the manuscript. J.R.Co. and J.W. researched data. B.R.B. designed experiments, researched data, and wrote the manuscript.

The authors thank Klaus Kaestner, University of Pennsylvania, for valuable discussions regarding the experimental design. The authors also acknowledge Tobias Raabe from the Penn Gene Targeting Core for preparation of murine embryonic stem cells; Jean Richa from the Penn Transgenic and Chimeric Mouse Facility for blastocyst injections; Heather Collins of the University of Pennsylvania Radioimmunoassay and BoiMarkers Core, for performing radioimmune assays; Ravindra Dhir and director Rex Ahima of the Penn Mouse Phenotyping, Physiology, and Metabolism Core; Changhong Li and Nicolai Doliba for help with calcium-imaging experiments; and Daniel Martinez and Edward Williamson from the Children's Hospital of Philadelphia Pathology Core for pancreatic sectioning and subsequent confocal microscopy.

Parts of this study were presented in abstract form at the 69th Scientific Sessions of the American Diabetes Association, New Orleans, Louisiana, 5–9 June 2009.

REFERENCES

1. Zhu Y, Xu G, Patel A, McLaughlin MM, Silverman C, Knecht K, Sweitzer S, Li X, McDonnell P, Mirabile R, Zimmerman D, Boyce R, Tierney LA, Hu E, Livi GP, Wolf B, Abdel-Meguid SS, Rose GD, Aurora R, Hensley P, Briggs M, Young PR. Cloning, expression, and initial characterization of a novel cytokine-like gene family. *Genomics* 2002;80:144–150
2. Cao X, Gao Z, Robert CE, Greene S, Xu G, Xu W, Bell E, Campbell D, Zhu Y, Young R, Trucco M, Markmann JF, Naji A, Wolf BA. Pancreatic-derived factor (FAM3B), a novel islet cytokine, induces apoptosis of insulin-secreting beta-cells. *Diabetes* 2003;52:2296–2303
3. Cao X, Yang J, Burkhardt BR, Gao Z, Wong RK, Greene SR, Wu J, Wolf BA. Effects of overexpression of pancreatic derived factor (FAM3B) in isolated mouse islets and insulin-secreting betaTC3 cells. *Am J Physiol Endocrinol Metab* 2005;289:E543–E550
4. Yang J, Gao Z, Robert CE, Burkhardt BR, Gaweska H, Wagner A, Wu J, Greene SR, Young RA, Wolf BA: Structure-function studies of PANDER, an islet specific cytokine inducing cell death of insulin-secreting beta cells. *Biochemistry* 2005;44:11342–11352
5. Burkhardt BR, Greene SR, White P, Wong RK, Brestelli JE, Yang J, Robert CE, Brusko TM, Wasserfall CH, Wu J, Atkinson MA, Gao Z, Kaestner KH, Wolf BA. PANDER-induced cell-death genetic networks in islets reveal central role for caspase-3 and cyclin-dependent kinase inhibitor 1A (p21). *Gene* 2006;369:134–141
6. Robert CE, Wu J, Burkhardt BR, Wolf B. Transgenic mice overexpressing the novel islet specific cytokine, PANDER, exhibit glucose intolerance (Abstract). *Diabetes* 2005;54(Suppl. 1):A400
7. Yang J, Wang C, Li J, Burkhardt BR, Robert-Cooperman CE, Wilson C, Gao Z, Wolf BA. PANDER binds to the liver cell membrane and inhibits insulin signaling in HepG2 cells. *FEBS Lett* 2009;583:3009–3015
8. Yang J, Robert CE, Burkhardt BR, Young RA, Wu J, Gao Z, Wolf BA. Mechanisms of glucose-induced secretion of pancreatic-derived factor (PANDER or FAM3B) in pancreatic beta-cells. *Diabetes* 2005;54:3217–3228
9. Wang O, Cai K, Pang S, Wang T, Qi D, Zhu Q, Ni Z, Le Y. Mechanisms of glucose-induced expression of pancreatic-derived factor in pancreatic β-cells. *Endocrinology* 2008;149:672–680
10. Burkhardt BR, Yang MC, Robert CE, Greene SR, McFadden KK, Yang J, Wu J, Gao Z, Wolf BA. Tissue-specific and glucose-responsive expression of the pancreatic derived factor (PANDER) promoter. *Biochim Biophys Acta* 2005;1730:215–225
11. Burkhardt BR, Cook JR, Young RA, Wolf BA. PDX-1 interaction and regulation of the Pancreatic Derived Factor (PANDER, FAM3B) promoter. *Biochim Biophys Acta* 2008;1779:645–651
12. Varela GM, Antwi DA, Dhir R, Yin X, Singhal NS, Graham MJ, Crooke RM, Ahima RS. Inhibition of ADRP prevents diet-induced insulin resistance. *Am J Physiol Gastrointest Liver Physiol* 2008;295:G621–G628
13. Yang J, Wong RK, Park M, Wu J, Cook JR, York DA, Deng S, Markmann J, Naji A, Wolf BA, Gao Z. Leucine regulation of glucokinase and ATP synthase sensitizes glucose-induced insulin secretion in pancreatic beta-cells. *Diabetes* 2006;55:193–201
14. Li C, Najafi H, Daikhin Y, Nissim IB, Collins HW, Yudkoff M, Matschinsky FM, Stanley CA: Regulation of leucine-stimulated insulin secretion and glutamine metabolism in isolated rat islets. *J Biol Chem* 2003;278:2853–2858
15. Liu YJ, Tengholm A, Grapengiesser E, Hellman B, Gylfe E. Origin of slow and fast oscillations of Ca2+ in mouse pancreatic islets. *J Physiol* 1998;508:471–481
16. Gilon P, Jonas JC, Henquin JC. Culture duration and conditions affect the oscillations of cytoplasmic calcium concentration induced by glucose in mouse pancreatic islets. *Diabetologia* 1994;37:1007–1014
17. Eaton RP, Allen RC, Schade DS. Hepatic removal of insulin in normal man: dose response to endogenous insulin secretion. *J Clin Endocrinol Metab* 1983;56:1294–1300
18. Polonsky KS, Rubenstein AH. C-peptide as a measure of the secretion and hepatic extraction of insulin. Pitfalls and limitations. *Diabetes* 1984;33:486–494
19. Kindmark H, Pigon J, Efendic S. Glucose-dependent insulinotropic hormone potentiates the hypoglycemic effect of glibenclamide in healthy volunteers: evidence for an effect on insulin extraction. *J Clin Endocrinol Metab* 2001;86:2015–2019
20. Rudovich NN, Rochlitz HJ, Pfeiffer AF. Reduced hepatic insulin extraction in response to gastric inhibitory polypeptide compensates for reduced insulin secretion in normal-weight and normal glucose tolerant first-degree relatives of type 2 diabetic patients. *Diabetes* 2004;53:2359–2365
21. Yaekura K, Julyan R, Wicksteed BL, Hays LB, Alarcon C, Sommers S, Poitout V, Baskin DG, Wang Y, Philipson LH, Rhodes CJ. Insulin secretory deficiency and glucose intolerance in Rab3A null mice. *J Biol Chem* 2003;278:9715–9721
22. Kido Y, Burks DJ, Withers D, Bruning JC, Kahn CR, White MF, Accili D.

Tissue-specific insulin resistance in mice with mutations in the insulin receptor, IRS-1, and IRS-2. *J Clin Invest* 2000;105:199–205
23. Brüning JC, Winnay J, Bonner-Weir S, Taylor SI, Accili D, Kahn CR. Development of a novel polygenic model of NIDDM in mice heterozygous for IR and IRS-1 null alleles. *Cell* 1997;88:561–572
24. Marie JC, Bailbé D, Gylfe E, Portha B. Defective glucose-dependent cytosolic Ca2+ handling in islets of GK and nSTZ rat models of type 2 diabetes. *J Endocrinol* 2001;169:169–176
25. Giroix MH, Sener A, Bailbe D, Leclercq-Meyer V, Portha B, Malaisse WJ. Metabolic, ionic, and secretory response to D-glucose in islets from rats with acquired or inherited non-insulin-dependent diabetes. *Biochem Med Metab Biol* 1993;50:301–321
26. Roe MW, Philipson LH, Frangakis CJ, Kuznetsov A, Mertz RJ, Lancaster ME, Spencer B, Worley JF 3rd, Dukes ID. Defective glucose-dependent endoplasmic reticulum Ca2+ sequestration in diabetic mouse islets of Langerhans. *J Biol Chem* 1994;269:18279–18282
27. Gupta RK, Vatamaniuk MZ, Lee CS, Flaschen RC, Fulmer JT, Matschinsky FM, Duncan SA, Kaestner KH. The MODY1 gene HNF-4alpha regulates selected genes involved in insulin secretion. *J Clin Invest* 2005;115:1006–1015
28. Sørensen H, Winzell MS, Brand CL, Fosgerau K, Gelling RW, Nishimura E, Ahren B. Glucagon receptor knockout mice display increased insulin sensitivity and impaired beta-cell function. *Diabetes* 2006;55:3463–3469